

PAPER

Control strategy to limit duty cycle impact of earthquakes on the LIGO gravitational-wave detectors

To cite this article: S Biscans *et al* 2018 *Class. Quantum Grav.* **35** 055004

View the [article online](#) for updates and enhancements.





IOP Astronomy ebooks

Part of your publishing universe and your first choice for astronomy, astrophysics, solar physics and planetary science ebooks.

iopscience.org/books/aas

Control strategy to limit duty cycle impact of earthquakes on the LIGO gravitational-wave detectors

S Biscans¹, J Warner², R Mittleman¹, C Buchanan³,
M Coughlin⁴, M Evans¹, H Gabbard⁵, J Harms⁶, B Lantz⁷,
N Mukund⁸, A Pele⁹, C Pezerat¹⁰, P Picart¹⁰, H Radkins²
and T Shaffer²

¹ LIGO, Massachusetts Institute of Technology, Cambridge, MA 02139, United States of America

² LIGO Hanford Observatory, Richland, WA 99352, United States of America

³ Department of Physics and Astronomy, Louisiana State University, Baton Rouge, LA 70803, United States of America

⁴ Department of Physics, Harvard University, Cambridge, MA 02138, United States of America

⁵ Albert-Einstein-Institut, Max-Planck-Institut für Gravitationsphysik, D-30167 Hannover, Germany

⁶ Università degli Studi di Urbino 'Carlo Bo', I-61029 Urbino, Italy

⁷ Stanford University, Stanford, CA 94305, United States of America

⁸ Inter-University Centre for Astronomy and Astrophysics (IUCAA), Post Bag 4, Ganeshkhind, Pune 411 007, India

⁹ LIGO Livingston Observatory, Livingston, LA 70754, United States of America

¹⁰ Le Mans Université, CNRS UMR 6613, 72085 Le Mans, France

E-mail: sbiscans@ligo.mit.edu

Received 14 July 2017, revised 28 November 2017

Accepted for publication 2 January 2018

Published 31 January 2018



Abstract

Advanced gravitational-wave detectors such as the laser interferometer gravitational-wave observatories (LIGO) require an unprecedented level of isolation from the ground. When in operation, they measure motion of less than 10^{-19} m. Strong teleseismic events like earthquakes disrupt the proper functioning of the detectors, and result in a loss of data. An earthquake early-warning system, as well as a prediction model, have been developed to understand the impact of earthquakes on LIGO. This paper describes a control strategy to use this early-warning system to reduce the LIGO downtime by $\sim 30\%$. It also presents a plan to implement this new earthquake configuration in the LIGO automation system.

Keywords: LIGO, earthquakes, control, seismic

(Some figures may appear in colour only in the online journal)

Introduction

The laser interferometer gravitational-wave observatory (LIGO) consists of two identical, 4 kilometer long interferometric detectors installed at the Hanford, Washington (H1) and Livingston, Louisiana (L1) sites in the United States. The detectors are Michelson interferometers with Fabry–Perot resonant cavity arms [1]. A prerequisite for the detectors to collect scientific data is that the cavities are held in optical resonance (lock) at their operating point [2]. Keeping the detectors locked is a complex task and large environmental disturbances can disrupt this process.

LIGO performed its first observation run (referred to as O1) from 18 September 2015 to 12 January 2016. During this period, the detectors were kept locked and the commissioning activities reduced to minimum. Environmental hazards such as earthquakes were one of the primary sources of disturbances (see table 1). According to the US Geological Survey (USGS), H1 experienced 265 earthquakes and L1 243 earthquakes of Richter magnitude 5 and greater while observing. All these events, independent of their epicenter location or depth, generated a non-negligible increase of the ground motion in the vertical and horizontal directions, from 10 mHz to 100 mHz, as illustrated by the seismic spectra in figure 1. This increase of the ground motion overwhelmed the LIGO seismic isolation system and prevented the detectors from operating. Loss of the interferometer lock occurred 62 times at Hanford and 83 times at Livingston during these earthquakes. Once the interferometer has lost lock, it can take hours to return to normal operation. As the number of detected astrophysical signals is proportional to the detector observing time, minimizing the detector downtime is of utmost importance. In this study we present a strategy that has the potential to significantly reduce LIGO downtime. While this work focuses on the Hanford detector, similar results are expected for the Livingston detector.

There is a direct correlation between the operating status of the interferometer and the ground velocity, as shown in figure 2(a): the interferometer becomes unstable at higher velocities. An earthquake mitigation scheme has been thus developed to limit the extra disturbance induced by earthquakes. The goal of this configuration is to maintain lock, even if doing so decreases the interferometer sensitivity to gravitational-wave sources. For this reason, it cannot be permanently activated and needs to be part of the LIGO automation system called Guardian [3].

The first section of this paper describes the LIGO interferometers and their seismic isolation systems in more detail. We then present the earthquake mitigation strategy and the expected performance it achieves. Finally, we explain how it will be integrated into the Guardian infrastructure in the future.

The LIGO detectors

The LIGO detectors are Michelson interferometers coupled with Fabry–Perot cavities in the arms. A beamsplitter is used to separate the input light into the two arms. A simplified optical layout of the LIGO detector is shown in figure 3. Each arm is comprised of an input test mass (ITM) and an output test mass (ETM) forming the Fabry–Perot arm cavity. Other cavities and auxiliary optics such as the power recycling mirror and the signal recycling mirror are present to enhance the signal quality [4].

Table 1. Detectors' status over the O1 period. Commissioning time represents the vital maintenance tasks needed to keep the interferometers running. Environmental disturbances encompasses earthquakes, high wind and storms.

	H1 (%)	L1 (%)
Observation	66	59
Commissioning	9	7
Environmental disturbances	17	24
Other	8	10

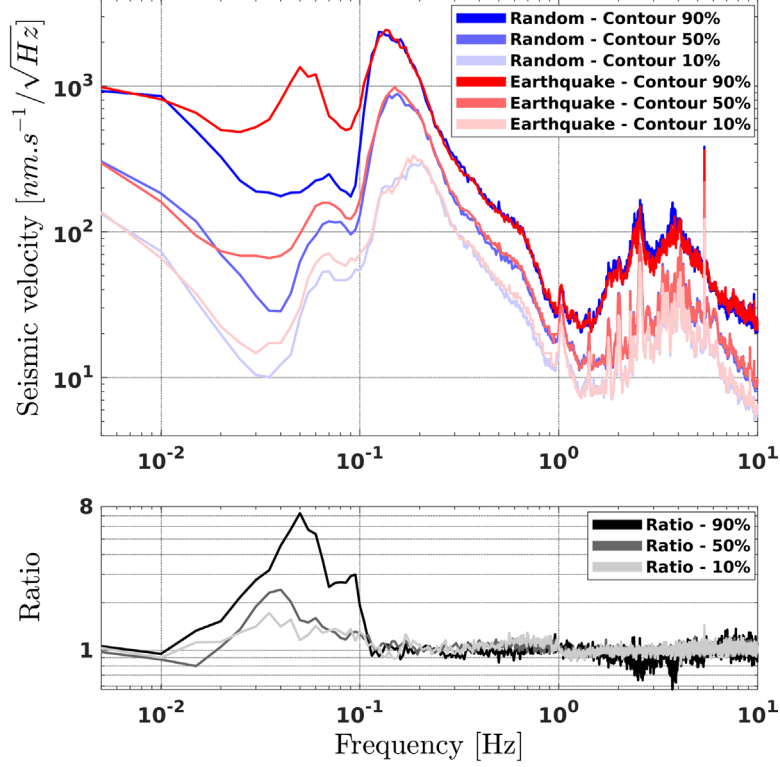


Figure 1. 1000 s long data stretches were selected over the total time span of the O1 period at H1. Specifically, the blue curves correspond to stretches selected at random times, while the red curves correspond to stretches selected during earthquakes of Richter magnitude 5 and above. For each frequency bin, the data were histogrammed and a set of probabilities was found. The different shades of color indicate different probability values (10%, 50%, 90%), the darker tone being a 90% probability. The bottom part of this figure represents the ratio between the red and the blue curves for each set. We observe a median amplification of the ground motion up to a factor of 2.4 in the (30 mHz–100 mHz) band. Only the horizontal direction along the Y-arm of the interferometer is represented here, but we obtain similar results in the X-horizontal direction and the vertical direction.

All the LIGO optics are mounted on seismic isolation platforms, which seek to decouple the optics from the ground. A hydraulic external pre-isolator (HEPI) is used as a pre-isolation and positioning stage outside the vacuum chamber. It supports an active internal seismic isolation (ISI) system inside the chamber, on which are mounted the optics. There are two types of

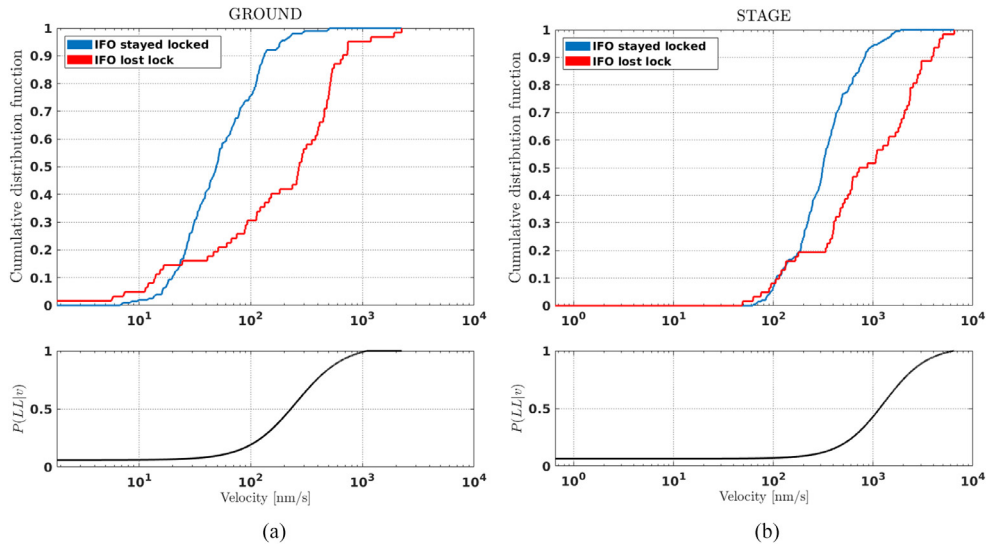


Figure 2. Comparison of Stage 1 ITM behavior in the (30 mHz–100 mHz) band for different ground motions: stretches selected during earthquakes when the interferometer survived (blue curve), stretches selected during earthquakes when the interferometer stops functioning (red curve). The top part of the figure represents the cumulative distribution function for the ground and the stage respectively, as a function of the peak velocity for each stretch. The plots indicate a direct correlation between velocity and the interferometer status. We observe a net increase of the stage velocity compared to the ground, due to a self-inflicted gain peaking in this frequency band. The bottom part of the plots represents $P(LL|v)$, the smoothed probability of losing lock as a function of peak velocity. It is computed by fitting the measured probability with a hyperbolic tangent function.

ISI systems: a single-stage platform and a two-stage platform. The single-stage platforms are used for the auxiliary optics in the small vacuum chambers called horizontal access modules (HAMs). The two-stage platforms are used for the core optics of the interferometer in the large vacuum tanks called basic symmetric chambers (BSCs). In total, a detector has 11 vacuum tanks (six HAM chambers, five BSC chambers) each with a seismic isolation platform. Despite some mechanical differences between the vibration isolation systems, the general concept is identical for all of them. A combination of active and passive isolation is provided to bring the BSC–ISI platform motion down to $1 \cdot 10^{-12} \text{ m } \sqrt{\text{Hz}}^{-1}$ at 10 Hz and the HAM–ISI platform motion down to $2 \cdot 10^{-11} \text{ m } \sqrt{\text{Hz}}^{-1}$ at 10 Hz.

The mechanics and functioning of these platforms have been extensively studied in previous works [5–7]. This paper will focus only on the active isolation configuration and performance of the BSC–ISI stage 1 platform. The BSC–ISI stage 1 platform is the only stage that has low noise Trillium T240 seismometers, which are used to mitigate low frequency disturbances. All the BSC–ISI platforms being identical, we chose to look at the ITM chamber of the Y arm (called ITMY) in the horizontal Y -direction. Figure 4 illustrates the layout of the BSC chamber.

The seismic platform control scheme

Each stage is equipped with a set of actuators, displacement sensors and inertial sensors. They are used to actively control the stage in the three translational and three rotational degrees of

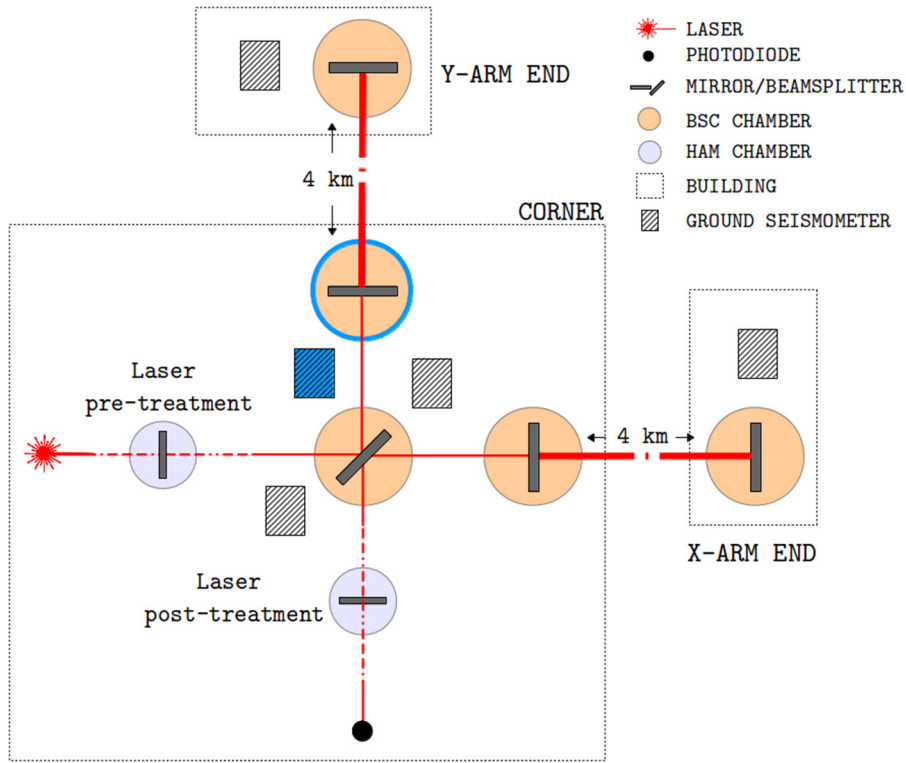


Figure 3. Simplified optical layout of the LIGO detector. *Laser pre-treatment* and *Laser post-treatment* represent all of non-core optics and the multiple vacuum chambers in which they are housed, including the power and recycling mirrors. The data presented in this study is extracted from the blue ground seismometer and the BSC chamber circled in blue (called ITMY).

freedom. The platforms have been designed to limit the cross-coupling between the different degrees of freedom, therefore, each degree of freedom can be actively controlled independently with single-input single-output compensators.

The LIGO seismic control scheme is a combination of feedback, feedforward and sensor correction. The block diagram in figure 5 shows the simplified control topology for one degree of freedom.

Feedback control

A control force F is used to reduce the inertial motion of the stage (Y_{Stage}), which is induced by the ground (Y_G). This control force is created using a combination of feedback and feedforward controllers. The feedback controller is fed by two sensors: a displacement sensor measuring the relative motion between the stage and the input motion ($Y_{\text{Stage}} - Y_G$), and an inertial sensor (seismometer) measuring the inertial motion of the stage (Y_{Stage}). Below 25 mHz, the seismometer noise becomes comparable to the ground motion, making inertial isolation impossible. Therefore, a displacement sensor is used at low frequencies and both sensors are blended together to feed the controller. The relative motion signal is low-passed by a filter L_{disp} , and the inertial motion signal is high-passed by a filter H_{in} . L_{disp} and H_{in} are designed to be complementary, meaning $L_{\text{disp}} + H_{\text{in}} = 1$. The frequency at which the low-pass and

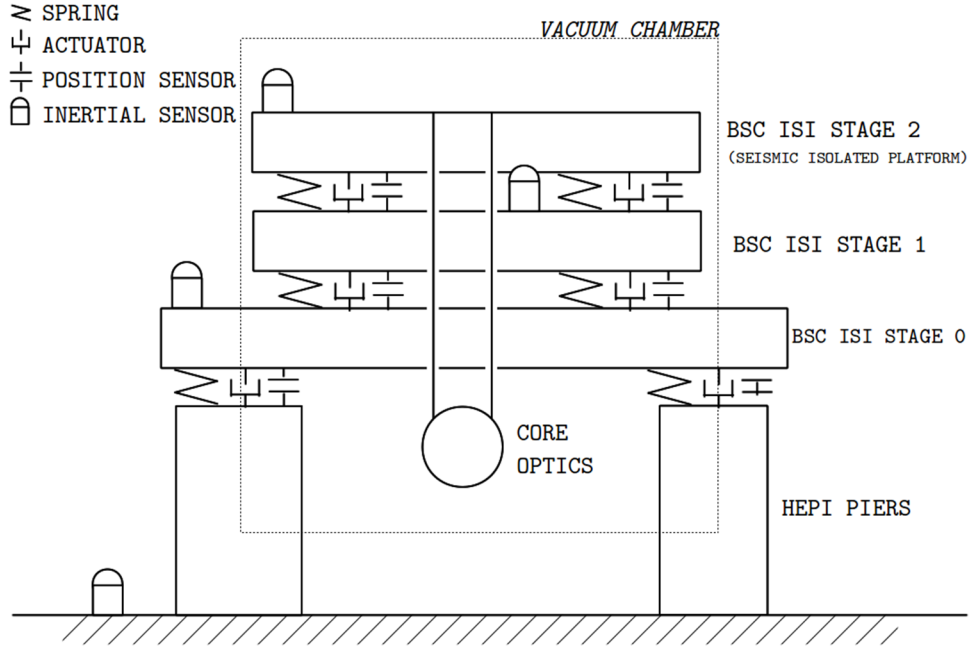


Figure 4. Schematic of a LIGO BSC chamber. Each stage is equipped with multiple actuators, position and inertial sensors (only a few are represented here for clarity). The core optics are supported by a quadruple pendulum (not shown for clarity) which provides additional seismic isolation in all degrees of freedom.

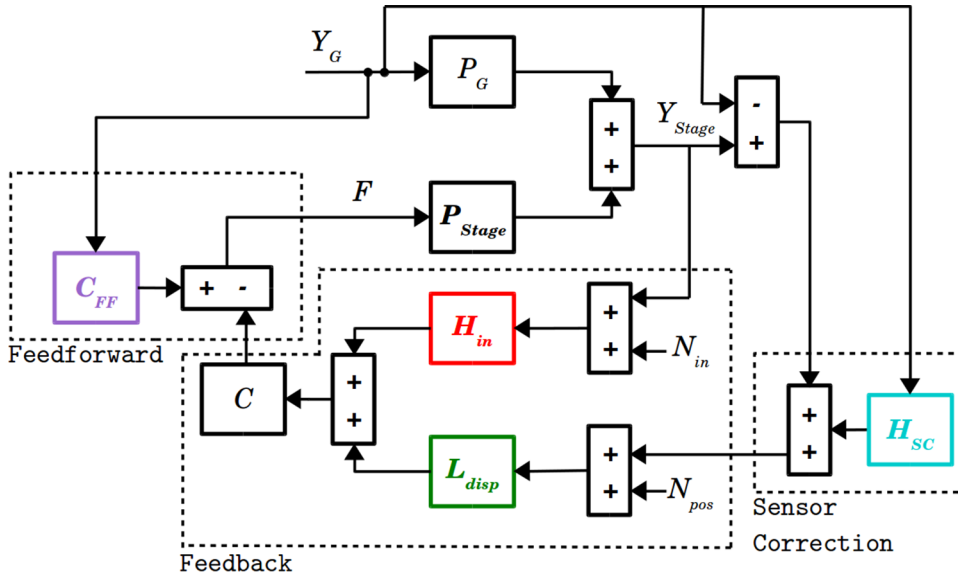


Figure 5. Control block diagram of a seismic isolation stage for one degree of freedom. The colored blocks are related to figure 6.

high-pass filters cross is called the blend frequency. The controller provides isolation up to 30 Hz, with high loop gain below 1 Hz. The expected inertial motion of the stage, when only the feedback control is engaged, is given by equation (1). N_{pos} and N_{in} represent the noise associated with the displacement sensors and inertial sensors respectively. P_G and P_{Stage} represent the transfer functions from the ground motion and applied force respectively.

$$|Y_{\text{Stage}}|^2 = \left| \frac{P_G + L_{\text{disp}}CP_{\text{Stage}}}{1 + CP_{\text{Stage}}} Y_G \right|^2 + \left| \frac{H_{\text{in}}CP_{\text{Stage}}}{1 + CP_{\text{Stage}}} N_{\text{in}} \right|^2 + \left| \frac{L_{\text{disp}}CP_{\text{Stage}}}{1 + CP_{\text{Stage}}} N_{\text{pos}} \right|^2. \quad (1)$$

Sensor correction

Sensor correction is a feedforward technique using a seismometer from the ground. The seismometer signal Y_G is filtered by H_{SC} and added to the position sensor signal ($Y_{\text{Stage}} - Y_G$) to create a virtual inertial sensor [8]. Our sensor correction is designed to maximize performance around 100 mHz. By adding the sensor correction to the feedback loop, the stage inertial motion becomes:

$$|Y_{\text{Stage}}|^2 = \left| \frac{P_G + L_{\text{disp}}CP_{\text{Stage}}(1 - H_{\text{SC}})}{1 + CP_{\text{Stage}}} Y_G \right|^2 + \left| \frac{H_{\text{in}}CP_{\text{Stage}}}{1 + CP_{\text{Stage}}} N_{\text{in}} \right|^2 + \left| \frac{L_{\text{disp}}CP_{\text{Stage}}}{1 + CP_{\text{Stage}}} N_{\text{pos}} \right|^2. \quad (2)$$

Feedforward control

A standard feedforward controller is added from the ground in parallel with the feedback and sensor correction loops. This operates where the coherence with the ground is high (above 1 Hz). Ultimately, the sensor correction and feedforward controllers are both feedforward techniques added to the feedback loop. However, these two controllers are implemented at different levels in the control scheme for technical reasons, as they target different frequency bandwidths. Overall, the stage absolute motion becomes:

$$|Y_{\text{Stage}}|^2 = \left| \frac{P_G + L_{\text{disp}}CP_{\text{Stage}}(1 - H_{\text{SC}}) + C_{\text{FF}}P_{\text{Stage}}}{1 + CP_{\text{Stage}}} Y_G \right|^2 + \left| \frac{H_{\text{in}}CP_{\text{Stage}}}{1 + CP_{\text{Stage}}} N_{\text{in}} \right|^2 + \left| \frac{L_{\text{disp}}CP_{\text{Stage}}}{1 + CP_{\text{Stage}}} N_{\text{pos}} \right|^2. \quad (3)$$

Equations (1)–(3) are plotted in figure 6. In this example, we used a BSC–ISI stage 1 model with the filters used during O1 to simulate the performance of each loop and the combined overall performance. The figure shows the transfer function between the stage and ground

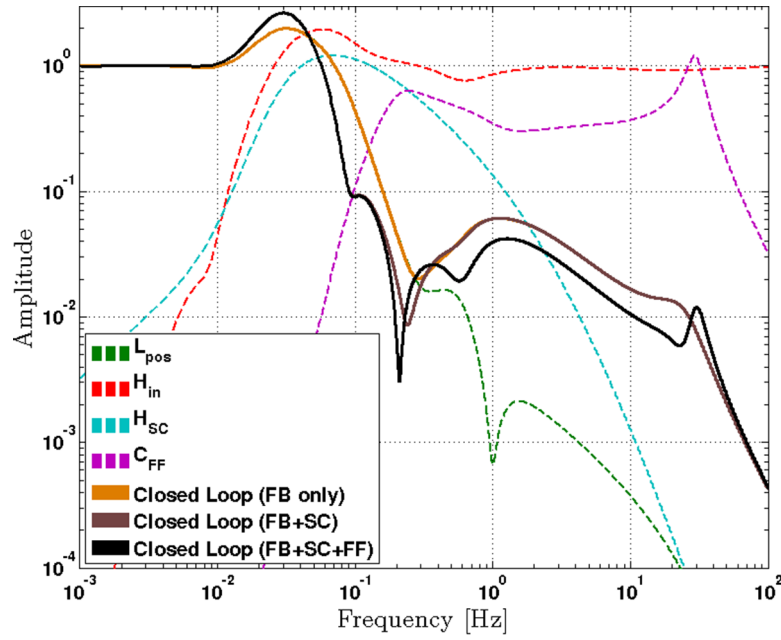


Figure 6. Example of the LIGO seismic control scheme performance on the BSC-ISI stage 1 platform. The dashed curves show the different filters used, as opposed to the solid curves showing the transfer functions from the ground motion with different loops engaged.

motion $\frac{Y_{\text{Stage}}}{Y_G}$ with the feedback loop only (solid orange curve), with the feedback loop and sensor correction on (solid brown curve) and with feedback, sensor correction and feedforward on (solid black curve). The motion associated with sensor noise is not represented on this figure for clarity. The open loop (not represented) has a 30 Hz unity gain frequency. The sensor correction filter (dashed cyan curve) is designed to provide extra isolation between 50 mHz and 200 mHz, whereas the feedforward filter (dashed purple curve) provides isolation at 1 Hz and above. At low frequencies where the loop gain is effectively infinite, the performance is limited by the low-pass filter (dashed green curve), and limited by the finite loop gain at higher frequencies. Typically, the low-pass filter is tuned to provide as much isolation as possible in the control bandwidth at the cost of some gain peaking around the blend frequency (in this case ~ 45 mHz). Below the blend frequency, the motion is dominated by the position sensor signal and the platform moves with the ground (transfer function of 1). Finally, some sharp notches are also present in the low-pass filter to target known payload resonances.

O1 filters

The filters used during O1 were designed to meet LIGO requirements and maximize the seismic isolation above 100 mHz, at the expense of some gain peaking at lower frequencies. The blue curve in figure 7 demonstrates the performance of this configuration at Hanford during a typical ground motion period. The stage provides a factor 38 of isolation at 200 mHz at the expense of a gain peaking of 4 at 54 mHz. While this gain peaking is not a limitation during typical ground behavior, it becomes problematic during an earthquake.

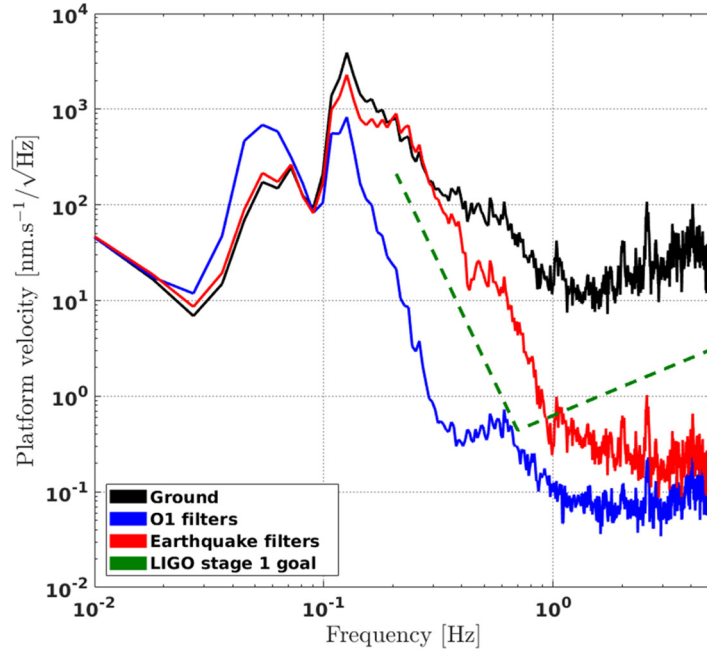


Figure 7. Seismic isolation provided by BSC-ISI stage 1 in the horizontal Y -direction at H1. The black curve represents a typical ground motion, and the blue curve the measured motion of the stage. The red curve is a simulation of the stage motion with the earthquake filters in place. The dotted curve indicates the LIGO goal to obtain from 200 mHz to higher frequencies for stage 1.

Figure 2 compares the performance of the stage during earthquakes. It shows a clear amplification of the ground motion by the stage over the bandwidth of interest (figures 2(a) versus (b)). The interferometer has a 50% chance of losing lock for a stage velocity higher than 1000 nm s^{-1} .

Earthquake filters

The goal of the earthquake control configuration is to find a balance between limited gain peaking at low frequencies (because the nominal gain peaking is at the frequency of maximum earthquake power) and performance at higher frequencies. At low frequencies, the loop gain is effectively infinite and the stage motion is directly dependent on the low-pass filter L_{disp} and the sensor correction filter H_{SC} , as demonstrated in equation (4). These two filters are tuned accordingly to reduce gain peaking, while the feedback and feedforward controllers stay untouched.

$$\lim_{\text{CP}_{\text{stage}} \rightarrow \infty} |Y_{\text{Stage}}|^2 = |(L_{\text{disp}}(H_{\text{SC}} - 1)Y_{\text{G}})|^2 + |H_{\text{in}}N_{\text{in}}|^2 + |L_{\text{disp}}N_{\text{pos}}|^2. \quad (4)$$

Figure 8 shows a comparison between the newly designed low, high and sensor correction filters with the O1 filters. To move the gain peaking out of the earthquake band, the blend

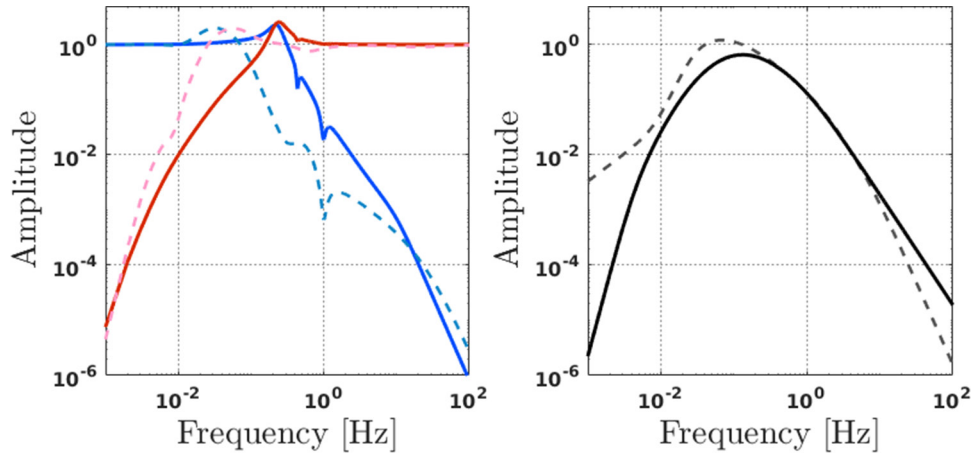


Figure 8. Comparison of the filters used during O1 (dashed lines) and the new designed filters for earthquakes (solid lines). The left part of the figure shows the complementary low-pass and high-pass filters. The right part shows the sensor correction filters.

frequency between the low-pass and the high-pass filters has been increased from 45 mHz to 250 mHz, and the sensor correction has been slightly modified to be less aggressive. Figure 7 shows the simulated stage 1 motion with the new earthquake configuration (red curve). In this case, the maximum gain peaking is reduced by a factor of 3.1. However, there is no longer any isolation at 200 mHz, which could be problematic for the detector. Seismic motion in the (100 mHz–300 mHz) frequency band is dominated by ‘secondary microseism’ [9], which consists of continuous traveling surface waves in the Earth’s crust. The sources of these waves are complex, but their amplitudes are associated with storms in the ocean. The proposed earthquake control configuration might not provide enough isolation to keep the detector locked if other disturbances like storms increase the ground motion around 200 mHz.

The lack of isolation between 200 mHz and 700 mHz could also limit gravitational-wave detection even if the interferometer stays locked. The increase of motion can get upconverted through the control chain to the mirror’s motion and affect LIGO sensitivity in the detection band. The green dashed curve in figure 7 shows the estimated maximum stage 1 motion allowed to not degrade LIGO designed sensitivity, and the new filters do not meet this requirement below 1 Hz. For these reasons, this configuration needs to be part of an automation system.

Automation system

It is important to switch to the new configuration only when a problematic earthquake arrives at the site. An early alert system called Seismon has been developed and installed at the observatories [10]. Seismon predicts the arrival time of the primary, secondary and surface waves of an earthquake with a few seconds accuracy, and with a notification latency of less than 10 min. This prediction uses data from a world-wide network of seismic observatories that has been compiled by USGS and can be accessed on the World Wide Web [11]. This gives enough time to switch the seismic configuration as needed.

The second role of Seismon is to predict, based on a logistic regression algorithm explained in [10], the likelihood of the interferometer to lose lock. Using this information and the current

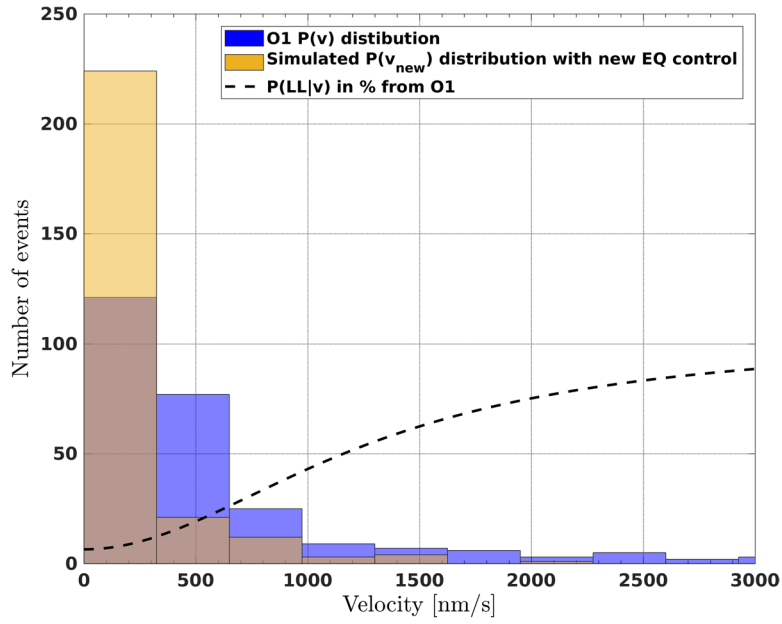


Figure 9. New $P(v_{\text{new}})$ distribution based on O1 data with $P(v_{\text{new}}) = \frac{P(v)}{1.5}$. As a reminder from figure 2, we plotted the probability of losing lock as a function of stage velocity $P(LL|v)$ in black.

state of the interferometer, a decision can be made on whether to trigger a change in the control configuration with the LIGO automation system.

Each interferometer is supervised by a state machine called the Guardian [3]. It consists of state machine automation nodes capable of handling control changes automatically. It is composed of multiple nodes, organised in a hierarchical fashion for each system and subsystem. In the case of the BSC-ISI, multiple intermediate states are required to bring the platform from the initial state to a fully isolated chamber. More states can be added to enable the switch between low-pass, high-pass and sensor correction filters. This change of state only requires a few minutes, as it is possible to switch these filters in either direction without having to turn off the isolation loops. This is due to a filter switching system which is already part of the LIGO infrastructure [12].

Improvement estimation

In this section we estimate the improvement in duty cycle due to reducing the sensitivity to earthquakes. Earthquake data collected during O1 is used to simulate the effect of the new earthquake filters on stage 1 velocity. We compare the averaged gain peaking induced by earthquakes in the (30 mHz–100 mHz) band between O1 filters and the earthquake filters. During O1, the isolation controls amplified the ground motion of earthquakes by a factor of 1.8 on average. With the new proposed filters, this amplification would be reduced to 1.2. Therefore, the stage velocity distribution in the (30 mHz–100 mHz) bandwidth will change from $P(v)$ to $P(v_{\text{new}})$, with $P(v_{\text{new}}) = \frac{1.2}{1.8}P(v) = \frac{P(v)}{1.5}$. Based on this new distribution (plotted in figure 9), and on the known probability of losing lock as a function of velocity $P(LL|v)$

(see figure 2), we can calculate the estimated number of lock-losses $P(LL)$ using Bayes' theorem, as written in equation (5). During O1, H1 lost lock 62 times because of earthquakes. With the new earthquake filters and stage velocity, we estimate only 42 lock-losses, meaning a $\sim 30\%$ reduction. Although this estimate has an uncertainty of $\pm 6\%$, it leads us to expect a significant improvement from this new configuration.

$$P(LL) = \sum_{\text{velocity bin}} P(LL|v)P(v_{\text{new}}). \quad (5)$$

Conclusion

In this paper, we have discussed the problem induced by earthquakes on the LIGO gravitational-wave detectors and presented a seismic control strategy to minimize their impact. We expect a $\sim 30\%$ improvement of the interferometers' robustness to earthquakes, which implies a direct increase in the number of detections for LIGO. We have shown that this configuration is not viable as a default configuration and needs to be part of a smart automation system. The LIGO automation infrastructure is capable of switching to these new filters based on early-warning predictions. This switching was not part of the LIGO second observation run and still has to be implemented. Further effort will be spent on integrating the presented strategy for the future observation runs.

Acknowledgments

The authors thank the LIGO Scientific Collaboration for access to the data and gratefully acknowledge the support of the United States National Science Foundation (NSF) for the construction and operation of the LIGO Laboratory and Advanced LIGO as well as the Science and Technology Facilities Council (STFC) of the United Kingdom, and the Max Planck Society (MPS) for support of the construction of Advanced LIGO. Additional support for Advanced LIGO was provided by the Australian Research Council.

ORCID iDs

S Biscans  <https://orcid.org/0000-0002-9635-7527>

J Harms  <https://orcid.org/0000-0002-7332-9806>

References

- [1] Abbott B *et al* 2016 Gw150914: the advanced LIGO detectors in the era of first discoveries *Phys. Rev. Lett.* **116** 131103
- [2] Staley A *et al* 2014 Achieving resonance in the advanced LIGO gravitational-wave interferometer *Class. Quantum Grav.* **31** 245010
- [3] Rollins J 2016 Distributed state machine supervision for long-baseline gravitational-wave detectors *Rev. Sci. Instrum.* **87** 094502
- [4] Aasi J *et al* 2015 Advanced LIGO *Class. Quantum Grav.* **32** 074001
- [5] Matichard F *et al* 2015 Seismic isolation of advanced LIGO: Review of strategy, instrumentation and performance *Class. Quantum Grav.* **32** 185003
- [6] Abbott R *et al* 2002 Seismic isolation for advanced LIGO *Class. Quantum Grav.* **19** 1591

- [7] Abbott R *et al* 2004 Seismic isolation enhancements for initial and advanced LIGO *Class. Quantum Grav.* **21** S915
- [8] Lantz B 2012 Description of the sensor correction FIR and IIR filter components (<https://dcc.ligo.org/LIGO-T1200285/public>)
- [9] Cessaro R 1994 Sources of primary and secondary microseisms *Bull. Seismol. Soc. Am.* **84** 142–8
- [10] Coughlin M *et al* 2017 Limiting the effects of earthquakes on gravitational-wave interferometers *Class. Quantum Grav.* **34** 044004
- [11] Data from the IRIS network of the USGS (available at <https://earthquake.usgs.gov/earthquakes/>)
- [12] Kurdyumov R, Kucharczyk C and Lantz B 2012 Blend switching user guide (<https://dcc.ligo.org/LIGO-T1200126/public>)